Microlensing Path Parameterization for Earth-like Exoplanet Detection around Solar-mass Stars

L. de Almeida, J. -D. Do Nascimento

The Astronomical Journal, 156:172 (6pp), 2018 October https://doi.org/10.3847/1538-3881/aadc68

Microlensing Path Parameterization for Earth-like Exoplanet Detection around Solar-mass Stars

L. de Almeida[1] and J.-D. do Nascimento, Jr.[1,2,3]
[1] Dep. de Física, Univ. Federal do Rio Grande do Norte, 59072-970 Natal, RN, Brazil; dealmeida.l@fisica.ufrn.br
[2] Harvard-Smithsonian Center for Astrophysics, 60 Garden St., Cambridge, MA 02138, USA
[3] Universit Paris-Sud, CNRS, Institut d'Astrophysique, Spatiale, UMR 8617, F-91405, Orsay Cedex, France
Received 2018 May 4; revised 2018 August 17; accepted 2018 August 20; published 2018 October 1

Abstract

We propose a new parameterization of the impact parameter u_0 and impact angle α for microlensing systems composed by an Earth-like exoplanet around a solar-mass star at 1 au. We present the caustic topology of such system, as well as the related light curves generated by using such a new parameterization. Based on the same density of points and accuracy of regular methods, we obtain results five times faster for discovering Earth-like exoplanets. In this big data revolution of photometric astronomy, our method will impact future missions like *WFIRST* (NASA) and *Euclid* (ESA) and their data pipelines, providing a rapid and deep detection of exoplanets for this specific class of microlensing event that might otherwise be lost.

Key words: gravitational lensing: micro – planetary systems – planets and satellites: detection

1. Introduction

Gravitational lensing of a point source creates two images with combined brightness exceeding that of the source. For small separation between the two images, the only observable consequence of the lensing is an apparent source brightness variation. This phenomenon is referred to as gravitational microlensing (Einstein 1936; Liebes 1964; Paczynski 1986; Mao & Paczynski 1991). Gravitational microlensing, among other things, is used as a constraint for several questions in astrophysics and cosmology, for example to study primordial black holes (Griest et al. 2011) and galaxy dark matter halo (Alcock et al. 1995). Simultaneously, the study of exoplanets has grown since the discovery of the first exoplanet orbiting a Sun-like star (Mayor & Queloz 1995), and among several branches, the study of habitability (Beaulieu et al. 2011; do Nascimento et al. 2016) has become one of the most active stellar astrophysics subjects. Currently, a new surprisingly successful application concerning microlensing is its capability to find the furthest and smallest planets outside the snow line region as compared to any other available extrasolar planets detection method (Gould & Loeb 1992; Bennett & Rhie 1996). The gravitational microlensing detections made so far present a variety of binary systems, and the detection sensitivity for the semimajor axis ranges from 0.5 au to 10 au, and the medium mass of the host star is $0.35\,M_{\odot}$ (Cassan et al. 2012). For these systems, the mass ratio, q, between the planet (m_2) and host star (m_1), $q = m_2/m_1$ is higher than 1×10^{-4}. To date, eight microlensing planets with planet-host mass ratio $q < 1 \times 10^{-4}$ have been characterized (Udalski et al. 2018). Gravitational microlensing is directly sensitive to the ratio of the masses of the planets and its host star, and the light curve gives us the projected apparent semimajor axis for the system normalized to the Einstein radius.

From the observational side, the surveys Microlensing Planet Search (MPS; Rhie 1999) and Microlensing Observations in Astrophysics (MOA; Rhie et al. 2000; Sumi et al. 2003) demonstrated for the first time that the microlensing technique is sensitive enough to detect Earth-mass exoplanets.

Shvartzvald et al. (2017) show that it is possible to detect an Earth-mass planet in a 1 au orbit around an ultracool dwarf, and Yee et al. (2009) present an extreme magnification microlensing event and its sensitivity to planets with masses as small as $0.2\,M_{\oplus} \simeq 2M_{\rm Mars}$ with projected separations near the Einstein ring (3 au). Gould et al. (2014) even showed the capability of the microlensing technique to discover Earth-mass planets around 1 au in binary systems. As discussed by Albrow et al. (2001), Gaudi et al. (2002), more than 77% of exoplanetary systems discovered with microlensing techniques show planets with masses lower than that of Jupiter and with semimajor axis between 1.5 and 4 au. These results are consistent with the fact that massive planets far away from their central stars are easier to detect with the microlensing method (Han 2006; Sumi et al. 2006). In this context, Paczynski (1986) shows that detection is a function of the impact parameter u_0 and the impact angle α. In this study, we propose a parameterization of the source's path to force it to cross the Caustic Region Of INterest (CROIN; Penny 2014). This offers an advantage for detecting Earth-like planets around solar-like stars during microlensing events.

In Section 2, we describe the lens equation and the semi-analytic method. We explore the caustic topology for events with a semimajor axis of about 1 au, with the lens at 7.86 kpc and source at 8 kpc, in Section 3 and explore the close systems topology geometry in Section 3.1 as well describe our parameterization proposal. We present light curves where it is possible to conduct an analysis of u_0 and α variation as a function of a fixed parameters in the lens-planet apparent separation in Section 3.2. We constructed a model to simulate our system based on a semi-analytical method for solving the binary-lens equation to take into account the source, lenses, caustic, critic curves, and producing images and light curves. We present our simulations and discuss our results in Section 4.

2. The Lens Equation

A gravitational microlensing event occurs when a star in the foreground (lens) passes near the line of sight of a background star (source) and thereby bends the source light from the original path. This bending of the light generates a relative magnification of the source, and if the system source-lens have relative movements, a characteristic light curve is produced. The deflection of the light by a single star can be expressed by $\alpha = \frac{4GM}{c^2 r}$, where α is the deflection angle, M the lens mass, G is the universal gravitational constant, c is the speed of light, and r is the impact parameter. If we establish D_S as the distance between the observer and the source and D_L as the distance between the observer and the lens, we can write the distance between the source and lens as $(D_S - D_L)$, and we can derive the well known equation of the Einstein radius

$$\theta_E = \sqrt{\frac{4GM}{c^2}\frac{D_S - D_L}{D_L D_S}}. \quad (1)$$

The Equation (1) holds regardless on the alignment between the source and the lens, but if they are aligned, we have the so called Einstein ring. Introducing the small distance β between the source and the lens, we can derive the lens equation for the single-lens case as $\beta = \theta - \frac{\theta_E^2}{\theta}$, which is the well known lens equation for the single-lens case, and it can be easily solved as a second-degree polynomial.

2.1. Formalism

For the binary-lens case, we can rewrite β, originally written for the single-lens case, using the complex notation to denote the lens equation for the two-lenses (Witt 1990; Witt & Mao 1995) case, representing a host star and their planet as

$$\omega = z - \frac{\varepsilon_1}{\bar{z} + \bar{z_1}} - \frac{\varepsilon_2}{\bar{z} + \bar{z_2}}. \quad (2)$$

In the above equation, ε_1 and ε_2 are the normalized lenses masses, with $\varepsilon_1 + \varepsilon_2 = 1$. The parameter z is the two-dimensional position written as the real and imaginary components of a complex number. The ω is the relative position of the source at a specific time. The bar over complex quantities indicates complex conjugation.

2.2. The Semi-analytic Method

Technically, to solve a lens equation with $n = 2$, it is necessary to invert a fifth-order polynomial and solve it to find the polynomial roots. To accomplish this task, we developed a model that uses a semi-analytic method to find polynomial coefficients and solutions (Witt 1990). For the case where the source is not close enough to the caustic-crossing region, we used the point-source magnification method to solve and obtain the light curve.

3. Earth-mass-like Systems Topology

Caustics modeling and microlensing critical event curves depends fundamentally on the apparent semimajor axis s between the lenses, i.e., the host lens and the planet. Here we used Einstein radius units R_E, and the mass fraction as $q = m_2/m_1$, where m_2 stands for the planet mass and m_1 mass of the star. The source's path is defined by two parameters, the impact parameter u_0 and the impact angle α. The impact parameter u_0 represents the closest distance between the source and the host lens at the time t_0.

In general, binary systems caustics produce close, resonant, and wide topologies (Schneider & Weiss 1987; Erdl & Schneider 1993), and with limits varying as a function of s and q. For this case, the impact angle α is the angle between the source trajectory and the x-axis of to the system. For the binary-lens case, the system lies in the x-axis.

For systems like our Sun–Earth system, in terms of Earth-Sun mass ratio, we find $q = 3 \times 10^{-6}$ and $s = 0.95969$, whereas the $m_1 = M_\odot$, $m_2 = M_\oplus$ and $1R_E = 1.0420$ au. In such a system, a planet orbiting a semimajor axis of 1 au would lie at the Einstein ring limit. Nevertheless, we cannot ignore possible values of $s < 1$ au due to the fact that for this system the semimajor axis is the projected separation between the planet and its host star. By considering systems with $q = 3 \times 10^{-6}$ and s as a free positive parameter, two topologies are more likely to be obtained, wide or close. As presented by Erdl & Schneider (1993), systems with such a wide topology satisfy the condition

$$s > \sqrt{\frac{\left(1 + q^{\frac{1}{3}}\right)^3}{1 + q}}. \quad (3)$$

For the interval $0.1 < s < 0.95969$, our system can only be close. Thus, to adjust the u_0 and α parameters in an efficient way, we need to know the position of the planetary caustic as a function of the s variation.

By analyzing Equation (3), we can conclude that a system with an Earth-Sun mass ratio can only be within a wide topology if $s > 1.0217R_E$. On the other hand, as our system can only assume $0.1R_E < s < 0.95969$, we can discard the wide topology for systems like our own. Thus, to use microlensing path parameterization for Earth-like exoplanet detections around solar-mass stars, a deep analysis of the close topology case is necessary.

3.1. Close Topology Case

The close topology is formed by three caustics. A central caustic close to the primary lens and two identical planetary caustics on either side of the system axis and opposite side of the planet. For a light curve of a source that passes close to the central caustic and on the same side as the planet, we are able to detect only the main lens signature. Following results by Erdl & Schneider (1993), we can define a such close topology system when the condition below is satisfied:

$$\frac{q}{(1+q)^2} < s^{-8}\left(\frac{1 - s^4}{3}\right)^3. \quad (4)$$

In the above equation, for $q = 3 \times 10^{-6}$, a system like our Sun–Earth system can only be close if $s < 0.9893$. In order to set the region of influence, we need at this point, to define the planetary caustic characteristics for close systems. Considering x as the position of the planetary caustic, this can be determined through the following equation (Han 2006):

$$X_{\rm pc} = \frac{1}{1+q}\left(s - \frac{1-q}{s}\right), \quad (5)$$

where $X_{\rm pc}$ is the the separation between the primary lens and the center of the planetary caustic. The Equation (5) makes

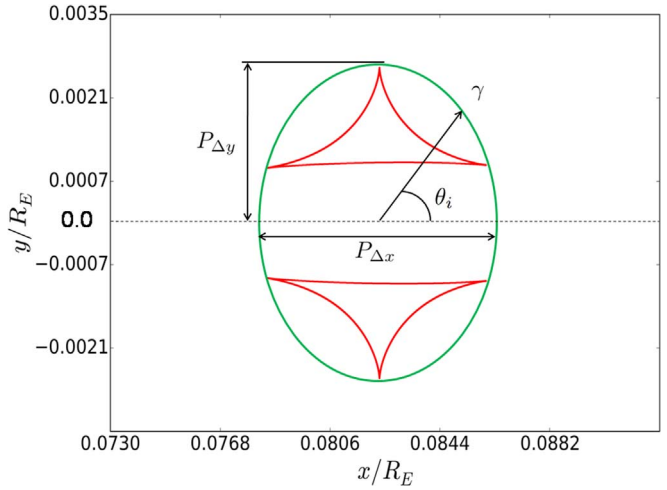

Figure 1. Planetary caustic in detail with $q = 3.003467 \times 10^{-6}$, $s = 0.9597E_R$, $u_0 = 0.0082E_R$. The green ellipse is the influence area defined by the Equation (10).

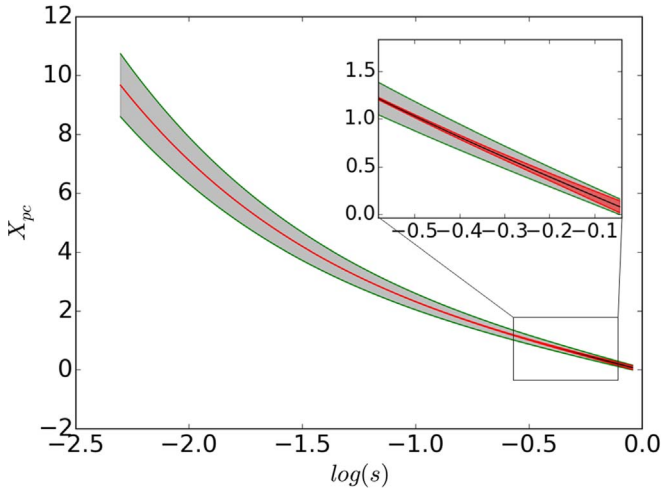

Figure 2. $X_{\rm pc}$ as a function of $\log s$ for our adopted system with $q = 3.003467 \times 10^{-6}$ and $0.95969 > s > 0.1$. The gray region is $2P_{\Delta y}$, and the red region is $P_{\Delta x}$ (both multiplied by twenty for better visualization).

clear that the smaller the value of s, the larger the value of $X_{\rm pc}$. By using this position $X_{\rm pc}$, we were able to parameterize some geometrical proprieties of the system and also set the dependency of the source's path with the localization of the influence region around the planetary caustic. We can also link the position $X_{\rm pc}$ of the planetary caustic center with the impact parameter u_0 by the following equation

$$u_0 = \frac{|s^2 + q - 1| \cdot |\tan(\alpha)|}{|q + 1| \cdot |s| \cdot \sqrt{\tan(\alpha)^2 + 1}}. \quad (6)$$

To better describe the entire region of interest, we need to geometrically describe the entire area containing the planetary caustic. For that, following the geometry of the problem, we found values for $P_{\Delta x}$ and $P_{\Delta y}$, (Figure 1) written below

$$P_{\Delta x} = \frac{3}{2} s^3 \sqrt{3}\, \sqrt{q}\,, \quad (7)$$

$$P_{\Delta y} = 2\frac{\sqrt{q}}{s\sqrt{s^2 + 1}}. \quad (8)$$

For close topologies in this regime, the planetary caustic can be enclosed by an ellipse independent of its size. Thus, the size of the influence area, which contains the planetary caustic, can be defined through an ellipse area πab, with $a = P_{\Delta x}/2$ and $b = P_{\Delta y}$. Thus, the influence area that defines the region containing the planetary caustic is

$$A = \pi \frac{P_{\Delta x}}{2} P_{\Delta y}. \quad (9)$$

Entering Equations (7) and (8) into Equation (9), we determined the area A that contains the planetary caustic as presented by the green ellipse in the Figure 1, and now as a function of q and s

$$A = \frac{\gamma^2 \pi s^2 \sqrt{3q}}{\sqrt{s^2 + 1}}, \quad (10)$$

where γ is a scalar factor for the size of the area that contains the planetary caustic. For the particular case of γ equal to 1, Figure 1, such an area fits the planetary caustic perfectly.

By analyzing Figure 2, we find that, for systems with close topology, the distance $X_{\rm pc}$ increases as s decreases. We can also see, based on Equations (7) and (8), that $P_{\Delta x}$ drastically decreases and $P_{\Delta y}$ increase when s approaches the origin. Equation (10) leads to the conclusion that the area of the planetary caustic overall decreases when s approaches to origin. Thus, even with $X_{\rm pc}$ getting bigger when s decreases, the total area is not enough for any possible detection. Figure 2 leads to the conclusion that $2P_{\Delta y}$ and $P_{\Delta x}$ approaches to same value when s approaches 1.

To link the source path with the *Caustic Region Of INfluence* (CROIN) as described by Penny (2014), we define all the points on the ellipse using the Equations (7) and (8) as

$$X_{\rm ip} = \gamma P_{\Delta x} \cos(\theta_i) + X_{\rm pc}, \quad (11)$$

$$Y_{\rm ip} = \gamma P_{\Delta y} \sin(\theta_i). \quad (12)$$

If we evolve θ_i from 0 to 2π in the equations above, we define the perimeter of the ellipse of area A, for the close topology case. Now, we can define the parameterization of the source path to the close topology case by the next equation

$$u_i = \frac{|\tan(\alpha) X_{\rm ip} - Y_{\rm ip}|}{\sqrt{\tan(\alpha)^2 + 1}}. \quad (13)$$

By setting $\gamma = 1$, and varying α from 0 to 2π, we obtain all values of u_0 from the Equation (13) with the path of the source always passing by the planetary caustic vicinity. Thus, to explore all of the possible light curves for our Earth-Sun model, we need to vary γ, α, and θ_i. Furthermore, we know from Paczynski (1986) that when analyzing a microlensing event, the parameters t_E, t_0, and u_0 are the first to be established from the single-lens model. It is more interesting here to parameterize α with respect to u_0, because the impact parameter u_0 is already set to a small error from the single-lens model. We note that Equation (13) is impossible to invert in terms of $\alpha(u_0)$, so we need to find another method to express the parameterization of α with respect to u_0.

To achieve that, we need to find a function $\alpha(u_0)$ that depends only on the position of interest given by $X_{\rm ip}$ and $Y_{\rm ip}$, and the impact parameter u_0. By analyzing the geometry (Figure 3), we get $d = (X_{\rm ip}^2 + Y_{\rm ip}^2)^{1/2}$, $\eta = a\cos(X_{\rm ip}/d)$ and $\varphi = a\cos(u_0/d)$. The impact angle α is $\psi - \pi/2$ with ψ being the sum of η and

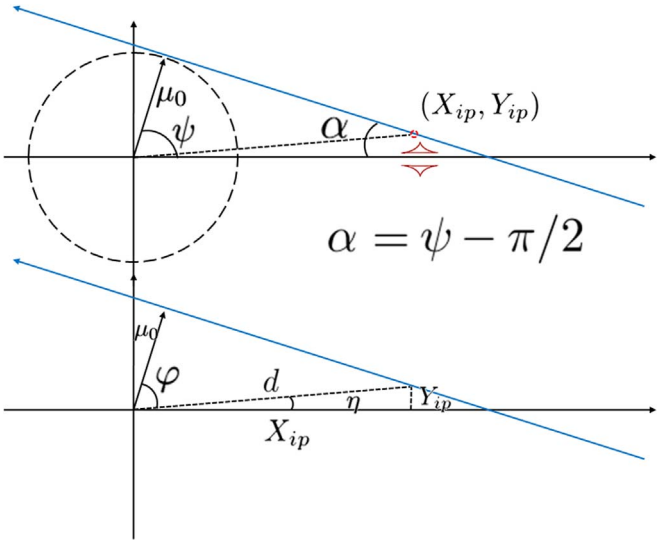

Figure 3. Top panel: topology of a close system showing the point of interest from Equations (18) and (19). Bottom panel: the geometry of the system with relative angles.

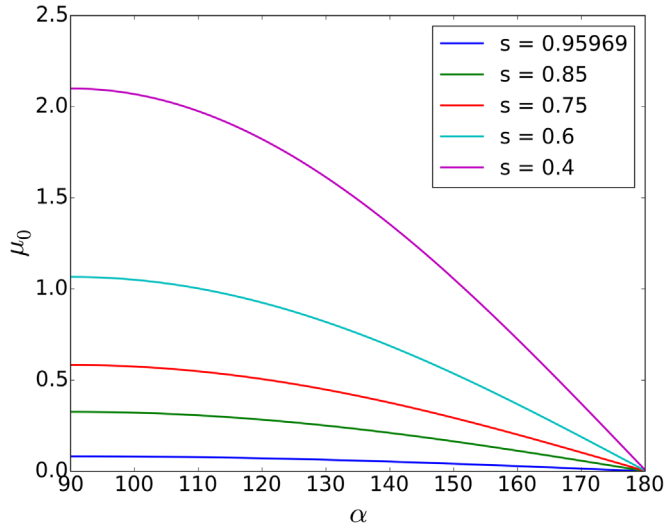

Figure 4. Evolution of the impact angle α when different initial mu_0 is set for $s = 0.95969$, 0.85, 0.75, 0.6 e 0.4.

φ. Then, we can simplify our new function α as:

$$\alpha(u_0) = a\cos\left(\frac{u_0}{\sqrt{X_{\rm ip}^2 + Y_{\rm ip}^2}}\right) - a\sin\left(\frac{X_{\rm ip}}{\sqrt{X_{\rm ip}^2 + Y_{\rm ip}^2}}\right). \quad (14)$$

Notice that Equation (14) depends solely on q, s, and u_0 and can fill the area of the planetary caustic by varying γ. This parameterization only covers the set of q and s that generate close topologies. For values out of this range (wide or resonant), we cannot use this parameterization. The evolution of the impact angle α was computed when different initial u_0 was set as $s = 0.95969$, 0.85, 0.75, 0.6, and 0.4. For all cases, the impact parameter u_0 must be smaller than the position of the planetary caustic or else the path of the source will not pass through the region of influence.

Figure 4 presents the evolution of the impact angle α when different initial u_0 is set to $s = 0.95969$, 0.85, 0.75, 0.6, and

Figure 5. Magnification map of a system with $q = 3.003467 \times 10^{-6}$ and $s = 0.9597E_R$. The color bar shows arbitrary values from low magnification (black) to high magnification (white).

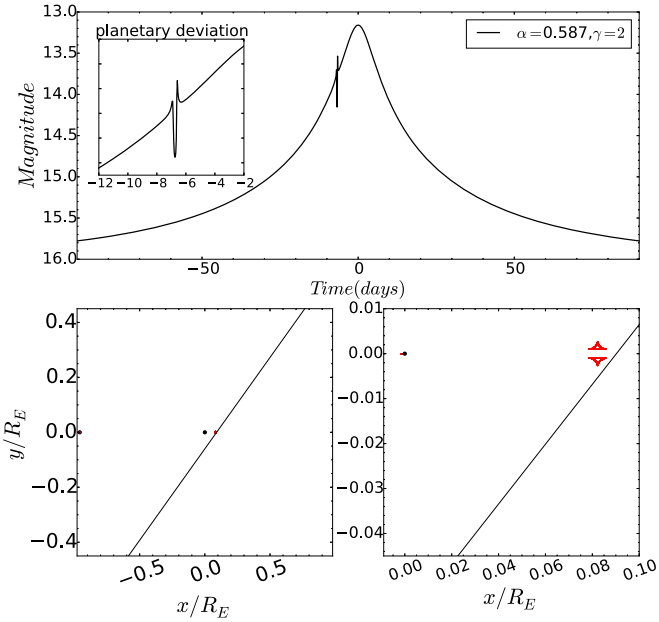

Figure 6. Top panel: light curve model for Sun–Earth system with $q = 3.003467 \times 10^{-6}$ and $s = 0.95969$ with a close-up at the planetary deviation. Bottom panel: the left panel shows a wide view of the system with the path in blue, and the right panel is a close-up of the planetary caustic.

0.4. We can see in all cases that the impact parameter u_0 must be smaller than the position of the planetary caustic or else the path of the source will not pass through the region of influence.

From Figure 4 and relative Equation (6), we see that as α approaches 90° (perpendicular with the lens axis), the value of u_0 increases. That happens because, in order for the source's path to cross the interest region in $X_{\rm pc}$, u_0 needs to be 0 so that $\alpha = 2\pi$ and if the path is perpendicular, with $\alpha = \pi/2$, then u_0 must be set to the value of $X_{\rm pc}$. According to Penny (2014), this kind of parameterization can greatly accelerate the simulation of light curves in the search for low-mass planets, but at the cost of passing by possible detections in unlikely topologies.

3.2. Light Curves for Close Systems

Once we have the parameterization of $\alpha(u_0)$ and $u_0(\alpha)$ with respect to the positions $X_{\rm ip}$ and $Y_{\rm ip}$, we can generate all the light curves within the region of interest by varying γ in the Equations (11) and (12). Figure 6 shows a light curve of a

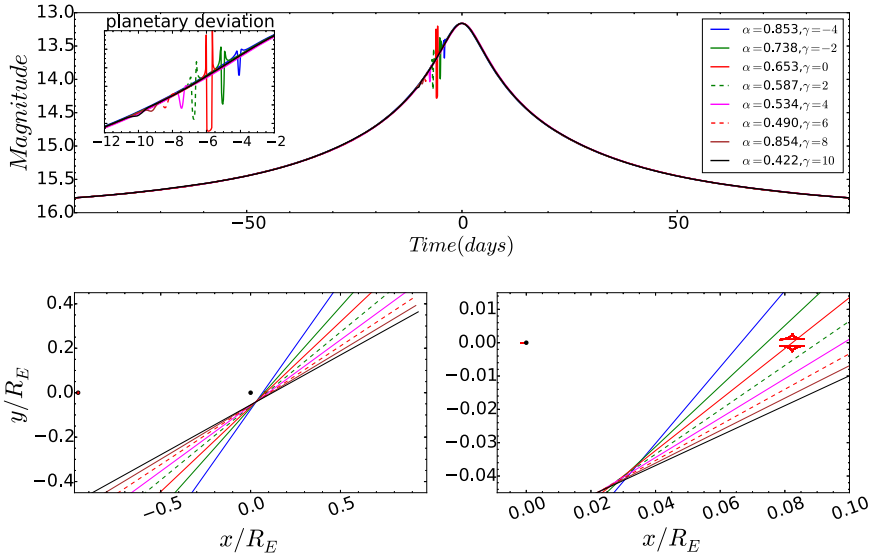

Figure 7. Top panel: eight superposed light curves with $-4 < \gamma 10$ for our simulated system; the planetary deviation panel shows a close-up at all the planetary signals. Bottom panels: the left panel shows the different source path for each γ on top of the topology of the system, and the right panel shows the planetary caustic region in close-up.

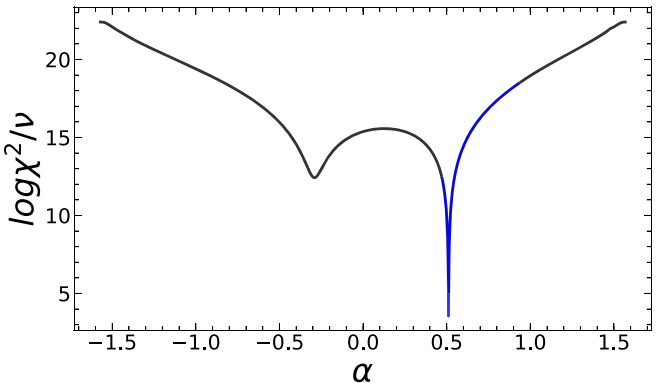

Figure 8. χ^2 diagram showing the reduced impact angle α. The blue line represents the search process by using our parameterization.

system that mimics our own Sun–Earth system with $q = 3.003467 \times 10^{-6}$, $s = 0.95969$ and path parameters as $u_0 = 0.15$, and $\alpha = 0.587$. We note a negative magnification at the planetary crossing region due to the source passing between the two planetary caustics. This negative magnification can be better visualized in Figure 5.

Figure 5 shows the magnification map of our system created by using a 5000×5000 pixels grid with arbitrary values for magnification. We can see that the central lens is responsible for almost all magnification of the source. The deviation due to the planetary caustic is negative between the two caustics but also presents a positive magnification at the crossing caustic regions.

By using the Equation (14) we generated several light curves by setting a fixed value for $u_0 = 0.15$ and varying γ from -4 to 10 thus, evolving the values of α from 0.422 (black line) to 0.853 (blue line). From our parameterization, we can see in Figure 7 that the overall aspect of the light curve for a single-lens case is preserved and that the end of all possible planetary deviations are superposing the same line. Thus, given the initial parameters t_0, t_E and u_0 from a single-lens approximation scenario, we are able to generate all possible light curves that could present a detectable planetary deviation. The detection itself depends on the observational cadence.

To demonstrate the computational efficiency and increase in the precision from our method, we performed a computational experiment and produced synthetic systems with the following parameters:

1. *cadence*: 24 daily photometric measurements.
2. *tobserv*: observational duration: 90 days.
3. *number of points*: cadence*tobserv.
4. *u*: impact parameter = 0.05.
5. *alpha*: inclination of impact = −2.489.
6. *q*: mass fraction = 3.003467e–6.
7. *s*: normalized projected separation = −0.95969.
8. *tE*: time in days to cross the Einstein radius = tobserv/2.

The experiment generates synthetic data with 4320 photometric points spread along 90 days and with a record every 1 hr. We apply a Gaussian noise error of 0.5% in the photometric measurement.

Based on the synthetic light curves, a systematic search for parameters was performed by setting q and s as our simulated system. Then, the same systematic search for parameters was performed by using our new parameterization. On the conventional method, we need to cover the dispersion of the q and s parameters, and we need also to cover the impact angle variation as $2\pi > \alpha > 0$. We set all other parameters as described above and a search now only on the α. The denser variation of α gives more accuracy to the result. We run the code to cover $2\pi > \alpha > 0$ with 1000 points. After that, we run the code using our model, varying the parameter γ from -5 to 8, with the same points quantity. We show in Figure 8 the comparative performance result between our method and the conventional one. In Figure 8, the blue line represents the search process by using our model. We can see that the search performed with the conventional model (black line) covers some unnecessary regions of the alpha domain. A second aspect is that in addition to region covered, we have less resolution in the regions of smaller χ^2. We see that α and u_0 parameterization with respect to CROIN forces the search to be

focused only in the region that it would be possible to detect our kind of interested system.

As far as the parameterization deals with a focused search process, its efficiency is mainly controlled by the ratio between the global search α (conventional model) and the focused one γ. Based on that, we conclude that, for this particular case, we arrive at the same result with a precision rate 5.2 higher and by using 1000 points in a range of 0.6 rad, instead of π on the conventional one. For the same density of points and accuracy, our method is five times faster at converging to the best fit, and this is one of its advantages.

4. Summary and Discussion

We analyzed a set of simulations constructed to search Earth-like exoplanets around solar -mass stars. Our simulations involved a parameter search on Sun–Earth models created using the semi-analytical method. We find that all solutions involving close topologies are not degenerated, since we are searching only around the region of interest. Our parameterization efficiency is mainly controlled by the ratio between the global search α and γ. Based on that, for our simulated case, we arrive at the same correct result with a precision rate that is 5.2 higher. For the same density of points and accuracy, our methods is five times faster. For a system with mass fraction and semimajor axis apparent similar to our Sun–Earth system and $t_E = 90$ days, we find that the planetary deviation takes about 1 day and can be observed by a high-cadence survey. The majority of microlensing events have typical timescales of about 20 days. LSST, with first light planed for 2019, does not plan to survey the bulge, but in any case, has enough cadence for about 0.25 days for field events and could in principle trigger follow-up observations to search for planets. *WFIRST* planed to be launched in 2024 has appropriated cadence and will observe the bulge and other fields.

We find that observed Sun–Earth analog systems will present a close topology (for semimajor axis close to 1 au) with doubled identical caustics on the other side of the planet. We also concluded that the ellipse around the planetary caustic decreases exponentially as s increases. We find that if the semimajor axis is equal to 1 au, then the deviation of the light curve from the single-lens case will last for about one day (for $t_E = 90$ days). The new values for $X_{\rm ip}$ and $Y_{\rm ip}$ are implemented within the new parameterization of $\alpha(u_0)$ and can easily be integrated in the parameters search, with γ dictating the evolution of α once we have defined a fixed u_0.

We would like to thank the anonymous referee, whose important suggestions greatly improved the paper. We thank CAPES and the Federal University of Rio Grande do Norte (UFRN) for financial support. J.D.N.Jr. acknowledges financial support by CNPq PQ 1D grant n°310078/2015-6.

ORCID iDs

L. de Almeida https://orcid.org/0000-0001-8179-1147
J.-D. do Nascimento, Jr. https://orcid.org/0000-0001-7804-2145

References

Albrow, M. D., An, J., Beaulieu, J. P., et al. 2001, ApJL, 556, L113
Alcock, C., Allsman, R. A., Axelrod, T. S., et al. 1995, PhRvL, 74, 2867
Beaulieu, J.-P., Bennett, D. P., Kerins, E., & Penny, M. 2011, in IAU Symp. 276, The Astrophysics of Planetary Systems: Formation, Structure, and Dynamical Evolution, ed. A. Sozzetti, M. G. Lattanzi, & A. P. Boss (Cambridge: Cambridge Univ. Press), 349
Bennett, D. P., & Rhie, S. H. 1996, ApJ, 472, 660
Bozza, V. 2000, A&A, 359, 1
Cassan, A., Kubas, D., Beaulieu, J.-P., et al. 2012, Natur, 481, 167
do Nascimento, J.-D., Jr., Vidotto, A. A., Petit, P., et al. 2016, ApJL, 820, L15
Einstein, A. 1936, Sci, 84, 506
Erdl, H., & Schneider, P. 1993, A&A, 268, 453
Gaudi, B. S., Albrow, M. D., An, J., et al. 2002, ApJ, 566, 463
Gould, A., & Loeb, A. 1992, ApJ, 396, 104
Gould, A., Udalski, A., Shin, I.-G., et al. 2014, Sci, 345, 46
Griest, K., Lehner, M. J., Cieplak, A. M., & Jain, B. 2011, PhRvL, 107, 231101
Han, C. 2006, ApJ, 638, 1080
Han, C., & Gould, A. 1995, ApJ, 447, 53
Liebes, S. 1964, PhRv, 133, 835
Mao, S., & Paczynski, B. 1991, ApJL, 374, L37
Mayor, M., & Queloz, D. 1995, Natur, 378, 355
Paczynski, B. 1986, ApJ, 304, 1
Penny, M. T. 2014, ApJ, 790, 142
Rhie, S. H. 1999, arXiv:astro-ph/9909433
Rhie, S. H., Bennett, D. P., Becker, A. C., et al. 2000, ApJ, 533, 378
Schneider, P., & Weiss, A. 1987, A&A, 171, 49
Shvartzvald, Y., Yee, J. C., Calchi Novati, S., et al. 2017, ApJL, 840, L3
Sumi, T., Abe, F., Bond, I. A., et al. 2003, ApJ, 591, 204
Sumi, T., Wozniak, P. R., Udalski, A., et al. 2006, ApJ, 636, 240
Udalski, A., Ryu, Y.-H., Sajadian, S., et al. 2018, AcA, 68, 1
Witt, H. J. 1990, A&A, 236, 311
Witt, J., & Mao, S. 1995, ApJ, 447, 105
Yee, J. C., Udalski, A., Sumi, T., et al. 2009, ApJ, 703, 2082